An Investigation into the Dynamic Interaction Between an Electro-dynamic Shaker and a Test Structure with Cubic Nonlinearity

Gianluca Gatti, Michael J. Brennan and Ivana Kovacic

Abstract This chapter describes the dynamic behaviour of a coupled system where a nonlinear oscillator is attached and driven harmonically by an electro-dynamic shaker. The shaker is modelled as a linear single degree-of-freedom oscillator and the nonlinear attachment is modelled as a hardening Duffing oscillator. The attachment consists of four elastic wires, represented as springs, and its nonlinearity is due to the geometric configuration of the springs, which incline as they extend. The mass of the nonlinear system is much less than the moving mass of the shaker so that the nonlinear system has little effect on the shaker dynamics. The objective is to explore the dynamic behaviour of this system under a range of different conditions. Of particular interest is the situation when the linear natural frequency of the nonlinear system is less than the natural frequency of the shaker such that the frequency response curve of the nonlinear system bends to higher frequencies and thus interacts with the resonance frequency of the shaker. It is found that for some values of the system parameters a two-part frequency response curve can occur: a closed detached curve can appear as a part of the overall amplitude-frequency response, and this detached curve can lie outside or inside the main continuous resonance curve.

1 Introduction

When a nonlinear oscillator is attached to a linear host structure, complex dynamics can occur [1, 2]. In particular, if it is assumed that the linear system is excited by a harmonic force, and that the responses of the two degree-of-freedom (DOF) system

G. Gatti
University of Calabria, 87036 Rende (CS), Italy
e-mail: gianluca.gatti@unical.it

M.J. Brennan
Universidade Estadual Paulista, 15385-000 Ilha Solteira (SP), Brazil
e-mail: mjbrennan0@btinternet.com

I. Kovacic (✉)
Faculty of Technical Sciences, University of Novi Sad, 21125 Novi Sad, Serbia
e-mail: ivanakov@uns.ac.rs

M. Belhaq (ed.), *Structural Nonlinear Dynamics and Diagnosis*,
Springer Proceedings in Physics 168, DOI 10.1007/978-3-319-19851-4_14

are predominantly harmonic at the frequency of excitation, multi-valuedness of the steady-state solution may occur, which affects the shape of the frequency response curve (FRC). Due to the coupling with the attachment, and for some particular combinations of the system parameters, the FRC can have interesting features, such as a detached resonance curve (DRC), lying inside or outside the main continuous FRC. Outer DRCs have been identified in several studies for the case of a purely nonlinear attachment with no linear stiffness term [3–7]. For the same condition, i.e. in the case when the attachment has a quasi-zero-stiffness (QZS) characteristic around the equilibrium position, inner DRCs may also appear with stable and unstable parts. These inner DRCs are of particular interest in this chapter.

For the sake of clarity, some assumptions are adopted in this study. The general aim is to limit the number of system parameters, so that on the one hand, their effect on the main features of the system dynamics are retained, and on the other hand, a quantitative insight is possible without additional cumbersome mathematical formulation. Further, it is assumed that the mass of the nonlinear attachment is small compared to that of the linear system. The effect of this assumption is that the nonlinear system does not have an appreciable effect on the vibration of the forced linear system. Although such an assumption is reasonable for the testing of a nonlinear attachment by a shaker, it excludes the nonlinear absorber as an application example. However, the interested reader can find more on this latter application in [8]. Regarding the type of excitation, it is assumed to be a harmonic force with a constant amplitude as frequency changes. With reference to the test of a nonlinear system using an electro-dynamic shaker, this implies that the shaker is supplied with a constant current at each frequency. This can easily be achieved in practice using commercially available shakers and controllers.

2 Mechanical and Mathematical Model

2.1 System Description

The practical system of interest in this chapter is depicted in Figs. 1 and 2. Photographs of the system are shown in Fig. 1a, b, and a schematic representation is shown in Fig. 2. A small mass m, is attached to a large shaker via a support frame, and the connection between the small mass and the support frame is made by four elastic wires, which can be modelled as four springs of stiffness k and a damper c. The initial tension in the wires can be adjusted upon assembly and has a profound effect on the stiffness of the system attached to the shaker. When the small mass vibrates in the horizontal direction, the springs stretch in tension, thus creating a geometric stiffness nonlinearity. The electro-dynamic shaker, which is used to excite the system, can be modelled as a linear system consisting of a parallel combination of a spring k_s and a damper c_s connected to a mass m_s, which is made up of the moving mass of the shaker and the support frame, and is much larger than the mass

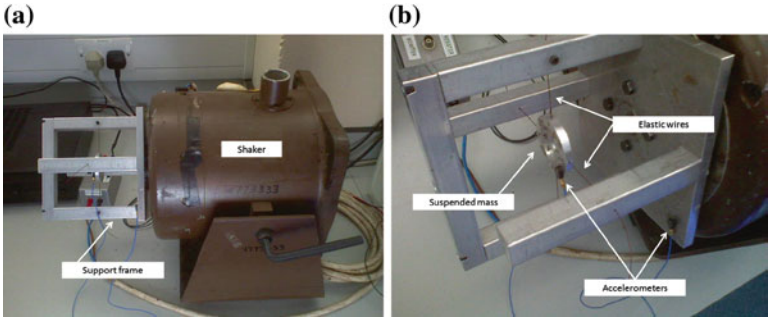

Fig. 1 Practical system under consideration, consisting of a nonlinear system attached to an electrodynamic shaker: **a** photograph of the system, **b** photograph showing the details of the nonlinear system attached to the shaker

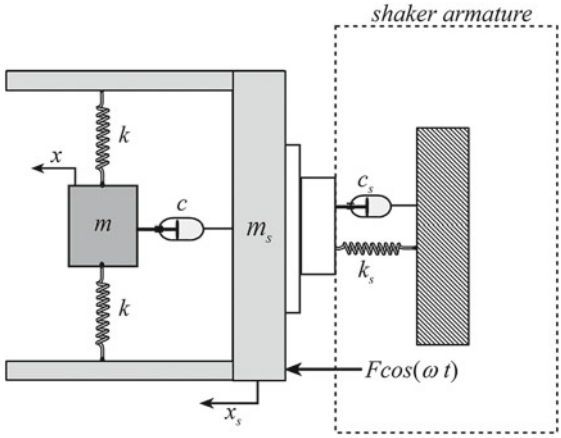

Fig. 2 Schematic view of the shaker and the nonlinear attachment

m. If the shaker is driven by a constant current at each frequency, the excitation can be modelled as a harmonic force with constant amplitude, $F\cos(\omega t)$ as shown in Fig. 2.

2.2 System Modelling

The wires connecting the small mass to the support structure can be modelled as shown in Fig. 3a. The distance d is equal to the length of the springs when they are assembled and the system is at rest. When the mass moves in the z direction, the springs incline to accommodate the motion as shown in the figure and it is the change in their length that causes the nonlinearity. Note that the effect of gravity on the mass is neglected. The relationship between the static restoring force f in Fig. 3a, and the resulting relative displacement z between the mass and the support structure, is given by

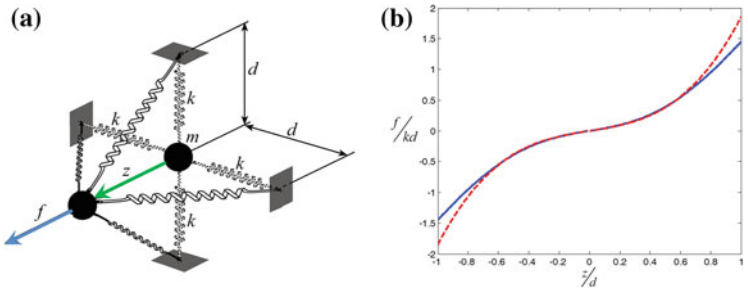

Fig. 3 Nonlinear system attached to the shaker: **a** schematic view; **b** non-dimensional restoring force as a function of the non-dimensional relative displacement for $d_0/d = 0.9$, exact expression (*solid line*), approximate expression (*dashed line*)

$$f = 4kz\left(1 - \frac{d_0}{\sqrt{z^2 + d^2}}\right), \tag{1}$$

where $d_0 \leq d$ is the length of the unstretched spring.

Using the McLaurin expansion to the third order for small z, (1) can be written as

$$f \approx k_1 z + k_3 z^3, \tag{2}$$

where $k_1 = 4k\left(1 - \frac{d_0}{d}\right)$ and $k_3 = 2k\frac{d_0}{d^3}$. The non-dimensional form of (1) and its approximation given by (2) are illustrated in Fig. 3b, for the particular case when $\frac{d_0}{d} = 0.9$. It can be seen that for a relative displacement $z = x_s - x$ less than about 40 % of the length d, the percentage error between (1) and (2) is less than 5 %. Furthermore, this error reduces for decreasing values of $\frac{d_0}{d}$.

Using the approximate expression for the spring restoring force, the equations of motion of the two DOF system depicted in Fig. 2 are given by

$$m_s\ddot{x}_s + c_s\dot{x}_s + k_s x_s + c\dot{z} + k_1 z + k_3 z^3 = F\cos(\omega t), \tag{3a}$$

$$m\ddot{x} - c\dot{z} - k_1 z - k_3 z^3 = 0 \tag{3b}$$

Equations (3a), (3b) correspond to the simplified system depicted in Fig. 4 and can be written in non-dimensional form as

$$y_s'' + 2\zeta_s y_s' + y_s + \mu y'' = \cos(\Omega\tau), \tag{4a}$$

$$w'' + 2\zeta w' + \omega_0^2 w + \gamma w^3 = y_s'' \tag{4b}$$

where $x_0 = F/k_s$ is the static displacement of the primary mass; $y_s = \frac{x_s}{x_0}$, $y = \frac{x}{x_0}$, $w = \frac{z}{x_0}$ are the non-dimensional displacement of the primary and secondary mass, and the corresponding relative displacement, respectively; $\omega_s = \sqrt{\frac{k_s}{m_s}}$, $\omega_1 =$

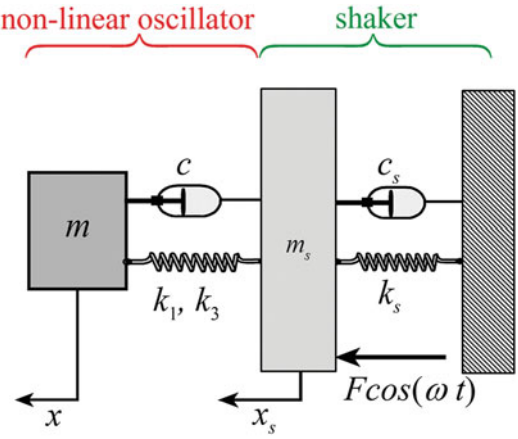

Fig. 4 Simplified model of the nonlinear system attached to the shaker

$\sqrt{\frac{k_1}{m}}$, $\omega_0 = \frac{\omega_1}{\omega_s}$ are the undamped natural frequency of the primary mass alone on its suspension, the linearized undamped natural frequency of the secondary mass alone on its suspension, and the ratio between the two, respectively; $\zeta_s = \frac{c_s}{2m_s\omega_s}$, $\zeta = \frac{c}{2m\omega_s}$ are the damping ratios of the primary and secondary masses, respectively; $\tau = \omega_s t$, $\Omega = \frac{\omega}{\omega_s}$, $\mu = \frac{m}{m_s}$ are the non-dimensional time, non-dimensional frequency and mass ratio, respectively; $\gamma = \frac{k_3}{\mu k_s} x_0^2$ is the nonlinear coefficient; and the primes denote differentiation with respect to the non-dimensional time.

It should be noted that a change in γ can be interpreted as a change in the nonlinearity or in the amplitude of excitation or in the mass ratio, or a combination of the three.

By assuming that the mass of the nonlinear attachment is small compared to that of the linear system, so that $\left|y_s''\right| \gg \left|\mu y''\right|$, as in the practical situation discussed, (4a), (4b) reduce to

$$y_s'' + 2\zeta_s y_s' + y_s = \cos(\Omega\tau) \tag{5a}$$

$$w'' + 2\zeta w' + \omega_0^2 w + \gamma w^3 = y_s''. \tag{5b}$$

Equation (5a) shows that the nonlinear system attached to the shaker has a negligible effect on the shaker vibration so that the shaker vibrates predominantly as a disconnected linear system, while (5b) describes a base-excited hardening Duffing oscillator [2].

3 Steady-State Response: Approximate Analytical Solution

3.1 Primary Resonance Response

Approximate solutions for the equations of motion given by (5a), (5b) are found in terms of the primary resonance responses, assuming that the system responds predominantly at the frequency of excitation, so that

$$y_s \approx Y_s \cos(\Omega\tau + \varphi_s), \tag{6a}$$

$$w \approx W \cos(\Omega\tau + \varphi) \tag{6b}$$

which also means that higher and lower order harmonics are negligible in the system response.

Substituting (6a), (6b) into (5a), (5b) and applying the harmonic balance method [9] results in

$$Y_s^2\left[\left(1-\Omega^2\right)^2 + 4\zeta_s^2\Omega^2\right] = 1 \tag{7a}$$

$$\frac{9}{16}\gamma^2 W^6 + \frac{3}{2}\gamma W^4\left(\omega_0^2 - \Omega^2\right) + W^2\left(\Omega^4 + 4\zeta^2\Omega^2 + \omega_0^4 - 2\omega_0^2\Omega^2\right) - \Omega^4 Y_s^2 = 0. \tag{7b}$$

Equations (7a), (7b) define the amplitude-frequency behaviour of the system response and show that the frequency response of the primary mass, is decoupled from the motion of the mass of the nonlinear attachment. This is due to the assumption adopted that the mass ratio is relatively small. However, (7b) is coupled with (7a) by the amplitude of the response of the primary mass Y_s.

The focus of this chapter is on the amplitude-frequency relationships only, so the expressions for the phases φ_s and φ in (6a), (6b) are not given.

Combining (7a) and (7b), gives the implicit amplitude-frequency equation, which can be written as

$$\frac{9}{16}\gamma^2 W^6 - \frac{3}{2}\gamma W^4\left(\Omega^2 - \omega_0^2\right) + W^2\left(\Omega^4 + 4\zeta^2\Omega^2 + \omega_0^4 - 2\omega_0^2\Omega^2\right) - \frac{\Omega^4}{\left[\left(\Omega^2-1\right)^2 + 4\zeta_s^2\Omega^2\right]} = 0. \tag{8}$$

Equation (8) is used to plot the FRC shown later in this chapter. It is interesting to note that, since it is cubic in W^2, this equation can yield up to three real solutions, and thus a multi-valued response for the steady-state can occur.

3.2 Stability

The stability of the steady-state solutions is calculated following the procedure in [9] and the limits for stability are determined to be

$$\Omega_{1,2} = \sqrt{\left(\frac{3}{2}W^2\gamma - 2\zeta^2 + \omega_0^2\right) \pm \sqrt{\left(-\frac{3}{2}W^2\gamma + 2\zeta^2 - \omega_0^2\right)^2 - \frac{27}{16}W^4\gamma^2 - \omega_0^4 - 3W^2\gamma\omega_0^2}}. \tag{9}$$

Both (8) and (9) involve a relationship between the amplitude of the non-dimensional relative displacement W and the non-dimensional frequency Ω. However, while (8) is an implicit polynomial equation whose roots can be solved numerically in terms of W for each value of Ω and of the system parameters, (9) is explicitly written in terms of Ω as a function of W and of the system parameters. Both (8) and (9) can then be plotted in the $\Omega - W$ plane. The solutions of (8) which are enclosed by the two curves given by (9) correspond to unstable solutions. In the FRCs plotted in this chapter, the unstable solutions are depicted by dashed lines while stable solutions are represented by solid lines.

4 Steady-State Response: Experimental Work

4.1 Setup Configuration

The experimental setup is depicted in Fig. 5. The electro-dynamic shaker was driven by a signal generator supplying a stepped-sine signal. Accelerometers were attached to the support structure and to the small mass, while a signal conditioner and a two-channel oscilloscope were used to observe the system response.

Before collecting data, two tests were carried out to broadly investigate the dynamic behaviour of the system. For each test, the support wires had a different initial tension. In the first test, a slow frequency sweep was applied from zero to

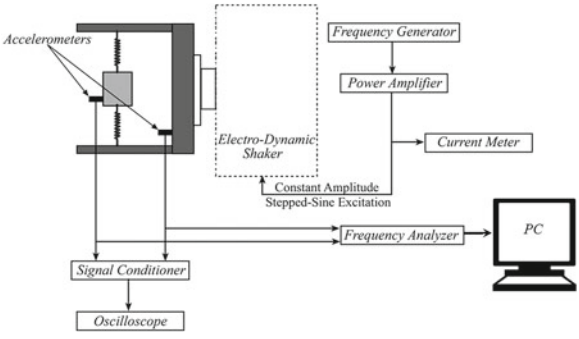

Fig. 5 Experimental set-up configuration

about 28 Hz and the response of the system was monitored using the oscilloscope. The first resonance was observed to be at about 19 Hz, with both masses vibrating with large amplitudes. As the frequency was increased beyond this, a second resonance occurred at about 26 Hz, in which only the vibration of the suspended mass was large. This was followed by a sudden decrease in the motion of the suspended mass (a jump-down). The frequency was then slowly swept down. A sudden increase in the amplitude was observed at a frequency of about 22 Hz, again for the suspended mass only (a jump-up). At about 19 Hz, the resonance response in which there was large motion of both the support structure and the suspended mass was observable. In the second test, similar behaviour was observed, but the jump-up and jump down frequencies were found to occur at about 29 and 34 Hz respectively.

To collect data, the shaker was then driven at discrete frequencies for the system with the wires set with low and high initial tension, corresponding to the cases described above, respectively. The excitation frequency was increased from 10 to 36 Hz, with a 1 Hz increment, and then decreased to 10 Hz with the same frequency increment. As mentioned previously, the amplitude of the excitation force was maintained at a constant level for all excitation frequencies, by manually adjusting the power amplifier so that the current was 0.8 A. At each frequency, once the system was at steady-state, five-second acceleration time histories were captured using a frequency analyser. Subsequently, these data were processed to give the displacement of the support structure and the suspended mass. The data are presented in terms of the absolute displacement x_s of the support structure and the relative displacement $z = x_s - x$ between the support structure and the suspended mass. The Fourier series coefficients are extracted from these two time histories and the amplitude of the first harmonic of each data set is plotted at the corresponding frequency. This can be seen in Fig. 6a, b for the system in which the springs have low initial tension, and in Fig. 6c, d for the high initial tension springs, respectively. The data points in each graph are denoted by a '+' for increasing frequency and a '×' for decreasing frequency.

In Fig. 6a, c, which depict the response of the support structure, it can be seen that, in each case, the FRC is similar, resembling the response of a single DOF linear system. The peak, at about 19.5 Hz corresponds broadly to the resonance frequency of the shaker and the attached mass of the support structure. It is evident, therefore, that the nonlinear system attached to the shaker has only a small effect on its response. This is because the combined mass of the moving part of the shaker and support structure is much greater than that of the suspended mass.

In the FRCs of the relative displacement Z, shown in Fig. 6b, d, in addition to the peak associated with the resonance frequency of the shaker, a jump-down and jump-up frequency can be seen, due to the response of the suspended mass. These are the frequencies where there is a sudden change in the amplitude of the response when the excitation frequency is changed very slowly [10]. The jump-down frequencies occur at approximately 26 and 33 Hz for the low initial tension and high initial tension cases, respectively, and the corresponding jump-up frequencies at about 21 and 31 Hz.

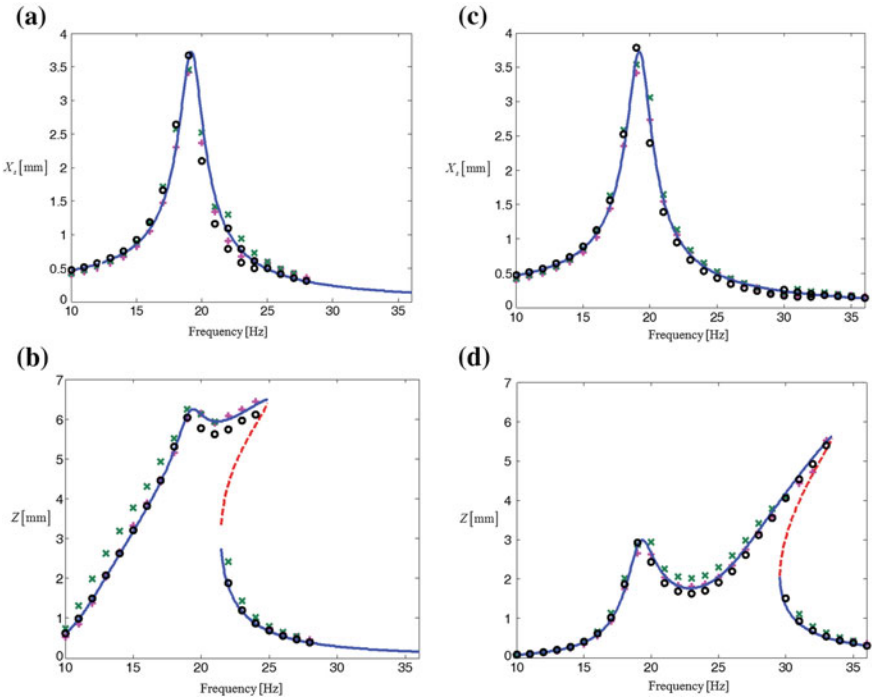

Fig. 6 Analytical, simulated and experimental results for step-sine input to the shaker: **a** and **b** wires with low initial tension; **c** and **d** wires with high initial tension. Analytical solution: stable solution (*solid line*), unstable solution (*dashed line*). Numerical solution ('○'). Experiment: increasing frequency ('+'), decreasing frequency ('×')

4.2 Parameter Estimation and Model Validation

To compare the experimental results with the predictions from the model, the system parameters are required. One group of parameters (m_s, k_s, c_s, m) was measured independently, and the other group (k_1, k_3, c) is considered to be unknown and chosen so that the FRCs are a best fit to the experimental data. Both sets of parameters are given in Table 1. The first group was estimated as follows. The combined mass of the moving part of the shaker and the support structure m_s, together with the stiffness k_s and damping c_s of the shaker were estimated through measurements made from an impact hammer test. With the suspended mass m detached and measured directly, the frequency response function (FRF) of the shaker and attached support structure was measured. The system parameters were estimated by fitting a theoretical single DOF FRF to the experimental FRF. Once these parameters were estimated, the electro-mechanical constant of the shaker, defined as the ratio of the force over the electric current (assumed to be constant), was estimated by measuring the FRF of

Table 1 System parameters for the two different experimental tests[a]

	m_s (kg)	c_s (Ns/m)	k_s (Ns/m)	M (kg)	c (Ns/m)	k_1 (N/m)	k_3 (N/m^3)	F (N)
Wires with low initial tension	1.72	19.12	2.51×10^4	19.4×10^{-3}	(0.234)	(1.3×10^2)	(1.1×10^7)	8.59
Wires with high initial tension	1.72	19.12	2.51×10^4	19.4×10^{-3}	(0.122)	(5.5×10^2)	(1.3×10^7)	8.59

[a]Numerical values in parenthesis are estimated by fitting the FRC to the experimental data

Table 2 Equivalent non-dimensional system parameters

	μ	ω_0	γ	ζ_s	ζ
Wires with low initial tension	0.011	0.677	4.6×10^{-3}	0.046	0.050
Wires with high initial tension	0.011	1.394	5.4×10^{-3}	0.046	0.026

the same system when driven by a random signal from the signal generator through the power amplifier. For a given input current of 0.8A, the force amplitude is calculated and is given in Table 1.

The second group of parameters is chosen to best fit the experimental data as follows. Noting that, for fairly weak nonlinearity, the damping has a negligibly small effect on the jump-up frequency and the corresponding FRC amplitude [11], a first two-parameter fit is performed to match those values, and k_1, k_3 are estimated. The remaining parameter c is then estimated by matching the jump-down frequency, which is affected by the degree of nonlinearity and damping. These three parameters are also listed in Table 1, but in parenthesis to indicate that they are estimated this way. For completeness, Table 2 lists the equivalent system parameters for the equation of motion written in the non-dimensional form of (4a), (4b).

Using the parameters in Table 2 and their relation to the dimensional parameters in Table 1, the FRCs described by (7a), (7b) are plotted in Fig. 6a–d together with the experimental results for comparison.

5 Steady-State Response: Numerical Solution

The FRCs reported in the section above are plotted using the approximate amplitude-frequency equations given in (7a), (7b), which are derived based on the assumption that the system response is predominately harmonic at the frequency of excitation. In this section it is shown how this assumption is verified and the analytical FRCs are validated.

The original equations of motion of the system, given in (4a), (4b), without the assumption for the mass ratio, are numerically integrated for a value of $\mu = 0.001$, which satisfies the assumption $|\mu \ddot{y}| \ll |\ddot{y}_s|$, and the Fourier series coefficients are extracted from the time history of the non-dimensional absolute displacement of the primary mass, y_s, and from the non-dimensional relative displacement between the primary and secondary mass, w. The amplitude of the first Fourier coefficient of the time response of w, which corresponds to the component at the frequency of excitation, is plotted as a circle in the FRCs shown in Fig. 6a–d. For the parameters of the experimental rig, higher- and lower-order harmonics are found to be negligible

compared to the first harmonic; the small differences between the analytical and numerical results around the resonances are due to the fact that the assumption $|\ddot{y}_s| \gg |\mu\ddot{y}|$ does not hold in these frequency regions. Examining Fig. 6a–d it can be seen that there is reasonably good agreement between the approximate analytical solution and the experimental results. Thus, the analytical model qualitatively captures the behaviour of the system.

Furthermore, for the numerical results superimposed on the FRCs reported in the figures of this chapter it is also verified that the amplitudes of the higher- and lower-order harmonics were negligible (less than 5 %) compared to that of the fundamental. A similar validation is performed on the time response of the displacement y_s. Although the FRCs of the corresponding amplitude are not reported here, a verification of the assumption is performed and, also in this case, it is valid for y_s.

6 Frequency-Response Curves for a QZS Attachment

The model developed in the previous sections is used here to investigate the effects of the system parameters on the FRC of the relative displacement W, and in particular on the interaction of the two resonances of the two DOF system depicted in Fig. 4. Of particular interest is the case where the natural frequency of the underlying linear system of the nonlinear attachment is lower than the natural frequency of the primary system. In this case, the FRC of the two DOF system will have a lower resonance frequency which is related to the nonlinear attachment and a higher resonance frequency which is related to the primary system. Due to the hardening characteristics of the nonlinear attachment, the bending of the first resonance peak to higher frequencies interacts with the second resonant peak, yielding the specific shape of the FRC. To limit the number of system parameters, the particular case is considered where the nonlinear attachment has a very small linear stiffness coefficient k_1, which can be practically achieved by a very low tightening of the suspension wires during assembly of the mechanical rig showed in Fig. 1. As a result, the non-dimensional frequency ratio is very small, i.e. $\omega_0 \approx 0$ and this corresponds to a QZS configuration around the equilibrium position [12]. For the results related to the case of the non-QZS configuration, the interested reader is directed to [13].

6.1 Effect of System Parameters: Jumps and Detachments

In this section, the FRCs of the non-dimensional relative displacement amplitude W are illustrated for some particular combinations of the systems parameters, in which ω_0 is set to zero, for the sake of simplicity. To this end, (8) is solved numerically for different values of frequency and for different combinations of the system parameters. The stability of the solution is checked by applying (9). The FRCs of the displacement amplitude of the primary mass, which are governed by (7a) are not shown here, since

this is assumed to be not affected by the nonlinear attachment, due to the assumption of the small mass ratio. The FRC of Y_s thus corresponds to the frequency response of a linear single DOF oscillating system.

In Figs. 7 and 8, two sets of sub-figures are reported, where the effect of the nonlinear parameter γ is shown for a similar value of the damping ζ_s in the primary system and two different values of the damping ζ in the attachment, respectively.

It can be seen from Figs. 7 and 8 that a variety of different shapes of the FRCs are obtained, depending on the values of the system parameters. In both figures, sub-figures a-f correspond to increasing values of the nonlinear parameter γ. It can be seen that the shapes of the FRCs in Figs. 7 and 8 are qualitatively the same, except for sub-plots c.

In particular, Figs. 7a and 8a refer to low values of the nonlinearity, and show a single-valued FRC which is qualitatively similar to that of a linear two DOF system with one of the stiffness equal to zero, since it is QZS. This shape is labelled as Type I (see the upper-right corner of the sub-figure). When the nonlinearity increases, an outer detached resonance curve, having a stable and an unstable branch, appear above the main continuous FRC. This shape is labelled as Type II. The detached resonance curve comes 'from above' in the sense that as the nonlinearity increases from zero to a specific value, it moves downwards until it merges with the main continuous curve. At this stage, two different types of behaviour may occur: the detached curve merges at $\Omega \approx 1$, which occurs in Fig. 7c; or it merges at $\Omega \approx 0$, which occurs in Fig. 8c. These two qualitatively different types of behaviour are labelled, respectively, as Type IIIa and IIIb. If the nonlinearity is increased further, the detached resonance curve appears inside the main continuous resonance curve, and this behaviour is again qualitatively similar for the sub-plots d in Figs. 7 and 8. The appearance of the inner detached resonance curve is associated with a FRC with a shape of Type IV. Such a detached curve decreases in size as the nonlinearity increases, as shown in sub-plots e, until it disappears. The shape of the FRC which is qualitatively similar to those shown in sub-plots f is labelled as Type V.

It is also interesting to note the typical bending of the resonance peak to the right (i.e. to higher frequencies), which is related to a hardening type nonlinearity. Such bending, which is clearly seen in the FRC of Type V, is associated with the jump frequencies. A lower jump-up frequency and a higher jump-down frequency are evident in the FRCs of the sub-plots f.

When an inner detached resonance curve appears, two new jump-up frequencies appear in the FRC, as shown in the sub-plots d and e. They are always lower than $\Omega = 1$. The outer detached resonance curves, shown in sub-plots b, appear above the main continuous FRC and introduce two jump-down frequencies, one of which corresponds to the frequency higher than $\Omega = 1$, while the other one corresponds to the frequency lower than $\Omega = 1$.

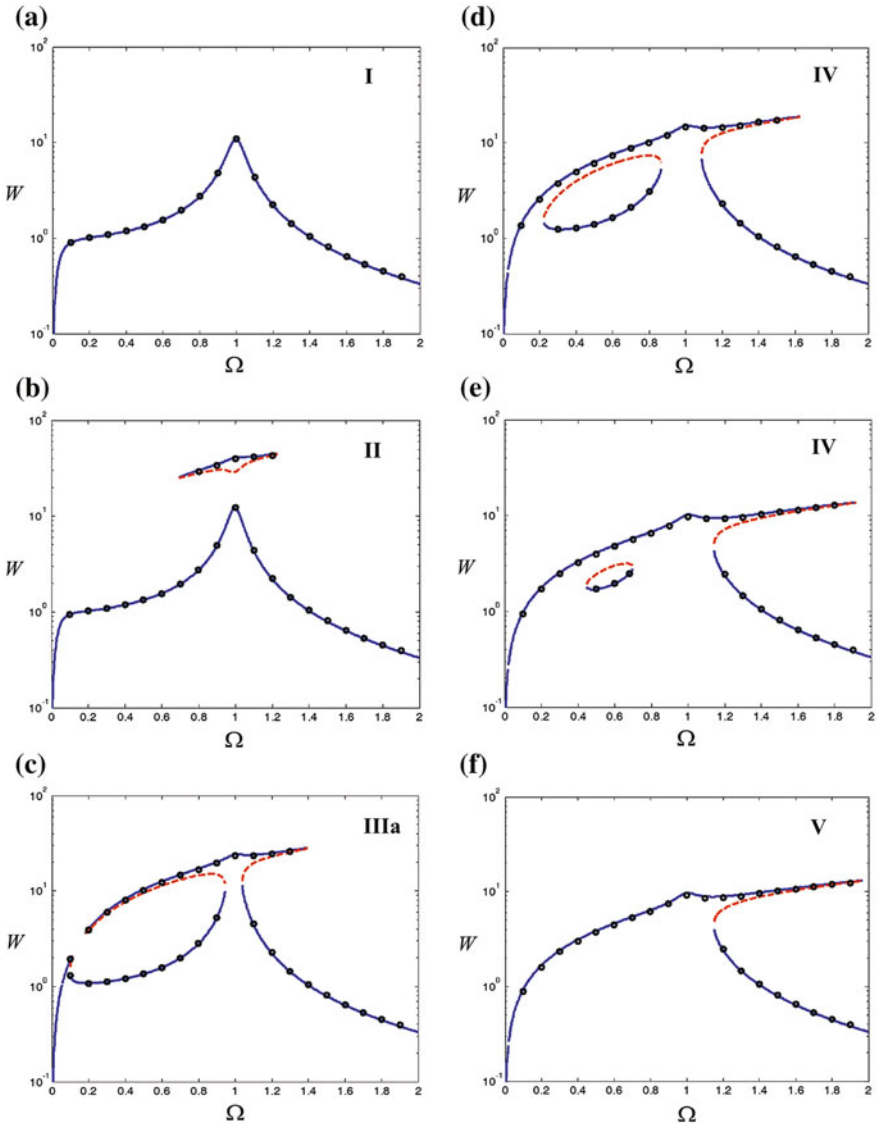

Fig. 7 FRCs of the normalized relative displacement W as a function of the normalized frequency Ω for $\zeta_s = 0.046$, $\zeta = 0.026$, and for different values of the nonlinear parameter γ: **a** $\gamma = 10^{-5}$; **b** $\gamma = 10^{-3}$; **c** $\gamma = 3.3 \times 10^{-3}$; **d** $\gamma = 10^{-2}$; **e** $\gamma = 2.6 \times 10^{-2}$; **f** $\gamma = 3 \times 10^{-2}$. Stable solutions (*solid lines*), unstable solutions (*dashed lines*). Numerical solution ('○')

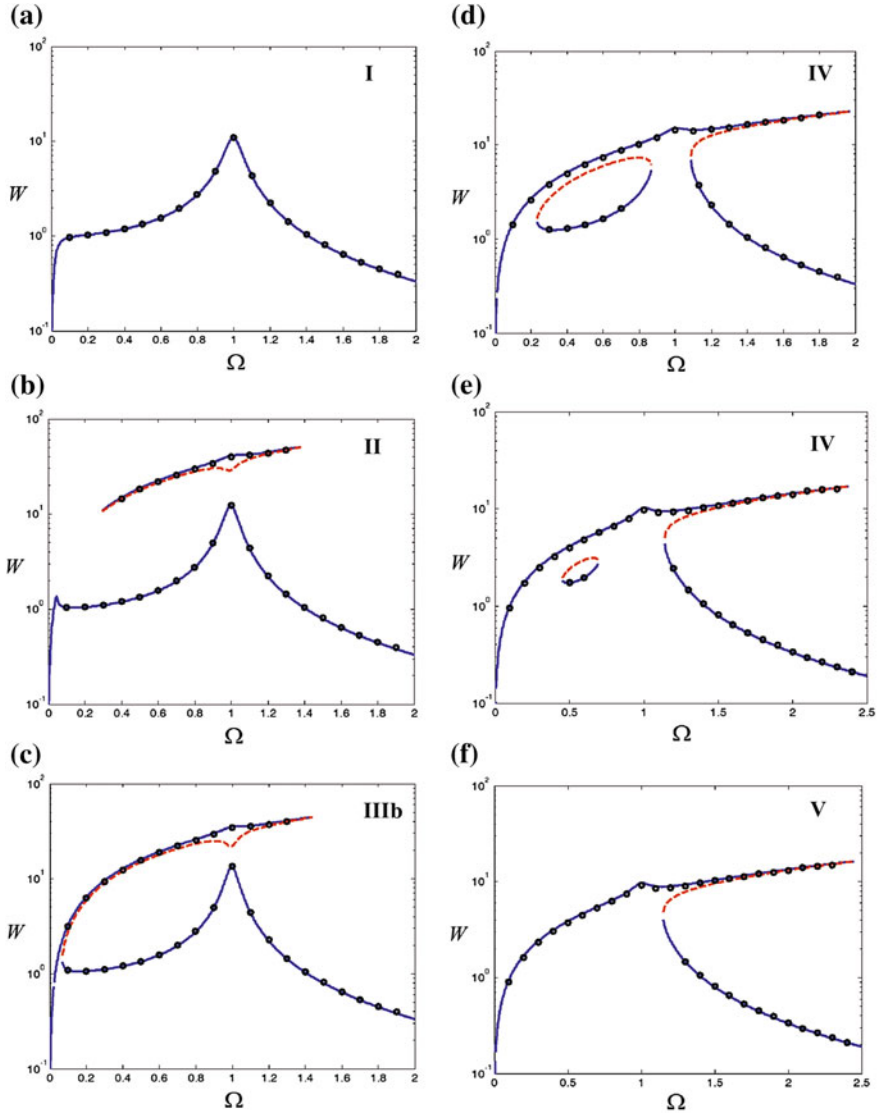

Fig. 8 FRCs of the normalized relative displacement W as a function of the normalized frequency Ω for $\zeta_s = 0.046$, $\zeta = 0.015$, and for different values of the nonlinear parameter γ: **a** $\gamma = 10^{-5}$; **b** $\gamma = 10^{-3}$; **c** $\gamma = 1.4 \times 10^{-3}$; **d** $\gamma = 10^{-2}$; **e** $\gamma = 2.6 \times 10^{-2}$;**f** $\gamma = 3 \times 10^{-2}$. Stable solutions (*solid lines*), unstable solutions (*dashed lines*). Numerical solution ('∘')

6.2 Insight into the FRC Shape

In this section a detailed analysis is performed with the aim of showing the effect of the system parameters on the shapes of the FRC and to categorize the main qualitative features. Again, for the sake of simplicity, the frequency ratio ω_0 is set to zero and (8) is rewritten as

$$\frac{9}{16}\gamma^2 W^6 - \frac{3}{2}\gamma W^4\Omega^2 + W^2\Omega^2\left(\Omega^2 + 4\zeta^2\right) - \frac{\Omega^4}{\left[\left(\Omega^2-1\right)^2 + 4\zeta_s^2\Omega^2\right]} = 0. \quad (10)$$

As mentioned earlier, (10) is cubic in W^2, and depending on the sign of the discriminant of the corresponding polynomial, it can yield up to three real solutions for the steady-state response of the system at a given excitation frequency. In particular, if its discriminant is negative, (10) has one distinct real root and a pair of complex conjugate roots; if it is positive, there are three distinct real roots; and if it is zero, then two roots coincide.

The transition between a single-valued and multi-valued response is determined by setting the discriminant to zero to get a quadratic equation in terms of the nonlinear parameter γ, and solving to give the following two solutions

$$\gamma_{u,l} = \frac{8}{81\Omega}\left[36\zeta^2\Omega + \Omega^3 \pm \left(\Omega^2 - 12\zeta^2\right)^{\frac{3}{2}}\right]\left[\left(\Omega^2-1\right)^2 + 4\zeta_s^2\Omega^2\right], \quad (11)$$

where the sub-scripts u and l stands for *upper* and *lower*, respectively. For values of the nonlinear parameter between γ_u and γ_l, the amplitude-frequency equation in (10) yields three distinct real solutions for the steady-state amplitude response W, while for values of γ equal to γ_u or γ_l, there are two coincident real solutions, and this occurs at the jump-up or jump-down frequencies. Thus, (11) give implicit expressions for the frequencies where a jump occurs. When (11) is plotted in the $\Omega-\gamma$ plane, the curves obtained are referred to as the *transition curves* or *bifurcation curves*. They are plotted in Figs. 9 and 10 to show the effects of the damping ratios in the linear and nonlinear oscillator. It can be seen that the transition curves are not defined for a value of the non-dimensional frequency lower than Ω_C, as indicated in the figures. Point C is obtained by setting $\gamma_u = \gamma_l$ in (11) to give

$$(\Omega_C, \gamma_C) = \left(2\sqrt{3}\zeta, \frac{128}{27}\zeta^2\left[\left(1-12\zeta^2\right)^2 + 48\zeta^2\zeta_s^2\right]\right). \quad (12)$$

It should be observed that Ω_C increases linearly with ζ and does not depend on ζ_s.

In particular, the bifurcation curves in Fig. 9 are shown for a fixed value of $\zeta = 0.03$ and for several values of ζ_s. It can be seen that a change in the value of ζ_s has the same effect on γ_u and γ_l, i.e. only shifting the position of the local minima of these curves, which occur approximately at $\Omega \approx 1$.

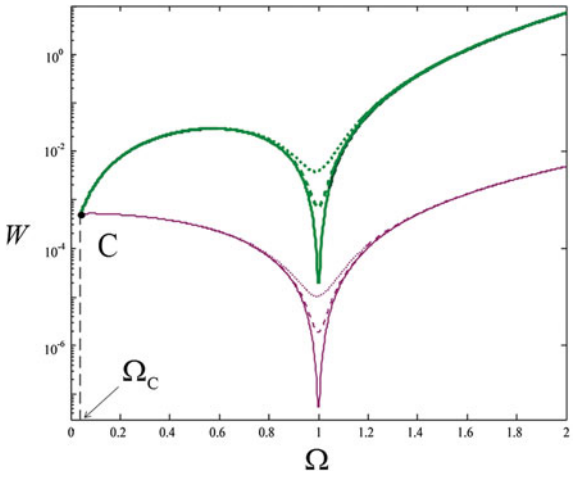

Fig. 9 Effects of the damping parameter ζ_s on the bifurcation curves depicted by a *thick line* (γ_u) and by a *thin line* (γ_l), for $\zeta = 0.03$: $\zeta_s = 0.005$ (*solid curve*); $\zeta_s = 0.03$ (*dash curve*); $\zeta_s = 0.07$ (*dot curve*)

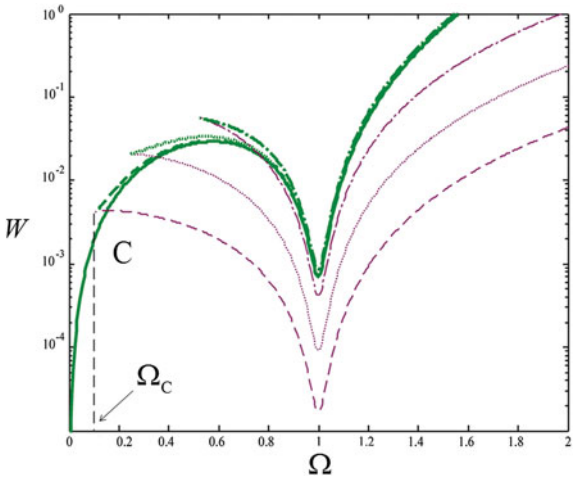

Fig. 10 Effects of the damping parameter ζ on the bifurcation curves depicted by a *thick line* (γ_l) and by a *thin line* (γ_l), for $\zeta_s = 0.03$: $\zeta = 0$ (*solid curve*); $\zeta = 0.03$ (*dash curve*); $\zeta = 0.07$ (*dot curve*); $\zeta = 0.15$ (*dash-dot curve*)

In Fig. 10, the transition curves are shown for a fixed value of $\zeta_s = 0.03$ and for different values of ζ. They illustrate that the damping in the attached nonlinear system has a different effect on γ_u andγ_l. It should be noted that, depending on the value of ζ, both curves can be with or without a local maximum point, which occurs at different frequencies, and may be with or without local minimum points, which occur at $\Omega \approx 1$. This local minimum of the upper curve is slightly affected by ζ.

It is also noted that if Ω_C is greater than unity, which occurs when $\zeta \approx 1/2\sqrt{3}$, no local maxima or minima exists, while in the special case when $\zeta = 0$, (11) reduce to $\gamma_l = 0$ and to

$$\gamma_u = \frac{16}{81}\left[\Omega^2\left(\Omega^2 - 1\right)^2 + 4\Omega^4\zeta_s^2\right]. \tag{13}$$

For the combination of parameters below this curve, depicted by the solid line in Fig. 10, three distinct real roots of (10) exist. In this case, point C coincides with the origin, and a multi-valued response occurs for any value of frequency.

Approximate relationships for the local maxima and minima of the bifurcation curves can be derived analytically by assuming that the damping in the linear oscillator is light, i.e. $\zeta_s \ll 1$. To this end, the local maxima on the upper and lower bifurcation curve are labelled as $\mathrm{U_{max}}$ and $\mathrm{L_{max}}$, respectively, while the local minima on the upper and the lower curve are labelled $\mathrm{U_{min}}$ and $\mathrm{L_{min}}$, respectively.

From Figs. 9 and 10, it can be observed that point C and point $\mathrm{L_{max}}$ are almost indistinguishable from each other, so that

$$\left(\Omega_{\mathrm{L_{max}}}, \gamma_{\mathrm{L_{max}}}\right) \approx \left(\Omega_{\mathrm{C}}, \gamma_{\mathrm{C}}\right) \approx \left(2\sqrt{3}\zeta, \frac{128}{27}\zeta^2\left(1-12\zeta^2\right)^2\right). \tag{14}$$

It can also be observed that the frequency corresponding to the relative maximum of the upper curve, $\mathrm{U_{max}}$, seems not to be greatly affected by either damping ratios. If these are then neglected in (11), a quadratic equation in terms of Ω^2 is obtained. This can be solved to give $\Omega = 1/\sqrt{3}$ and $\Omega = 1$, which correspond approximately to the frequencies where the maximum and minimum points of the upper transition curve occur. If the value $\Omega = 1/\sqrt{3}$ is substituted back into (11), the coordinates of point $\mathrm{U_{max}}$ in the $\Omega - \gamma$ plane are determined to be

$$\left(\Omega_{U_{\mathrm{max}}}, \gamma_{\mathrm{U_{max}}}\right) \approx \left(\frac{1}{\sqrt{3}}, \frac{32}{2187}\left[1+108\zeta^2+\sqrt{-\left(36\zeta^2-1\right)^3}\right]\right). \tag{15}$$

Finally, it can be noted that the frequency corresponding to the relative minima of the upper and lower curves appears at $\Omega \approx 1$. By substituting this value into (11), the coordinates of points $\mathrm{U_{min}}$ and $\mathrm{L_{min}}$ are obtained as

$$\left(\Omega_{U_{\mathrm{min}}}, \gamma_{\mathrm{U_{min}}}\right) \approx \left(1, \frac{32}{81}\zeta_s^2\left[1+36\zeta^2+\sqrt{\left(1-12\zeta^2\right)^3}\right]\right), \tag{16}$$

$$\left(\Omega_{L_{\mathrm{min}}}, \gamma_{\mathrm{L_{min}}}\right) \approx \left(1, \frac{32}{81}\zeta_s^2\left[1+36\zeta^2-\sqrt{\left(1-12\zeta^2\right)^3}\right]\right). \tag{17}$$

Points $\mathrm{U_{max}}$, $\mathrm{L_{max}}$, $\mathrm{U_{min}}$, $\mathrm{L_{min}}$ and C are used to define regions in the $\Omega - \gamma$ plane which characterize the different shapes of the FRCs. These are shown in Fig. 11a, b for two different combinations of ζ and ζ_s. Although Fig. 11a, b appear to be similar, they are different with respect to the relative positions of points $\mathrm{L_{max}}$ and $\mathrm{U_{min}}$. The characteristic regions where a specific shape in the FRC is achieved are indicated as I, II, IIIa, IV and V in Fig. 11a, and as regions I, II, IIIb, IV and V in Fig. 11b. They are also shaded by using different grey-scales. Each region in Fig. 11 is associated with the corresponding type of shape of the FRC, as indicated in the upper-right corners of Figs. 7 and 8 and discussed in the previous section.

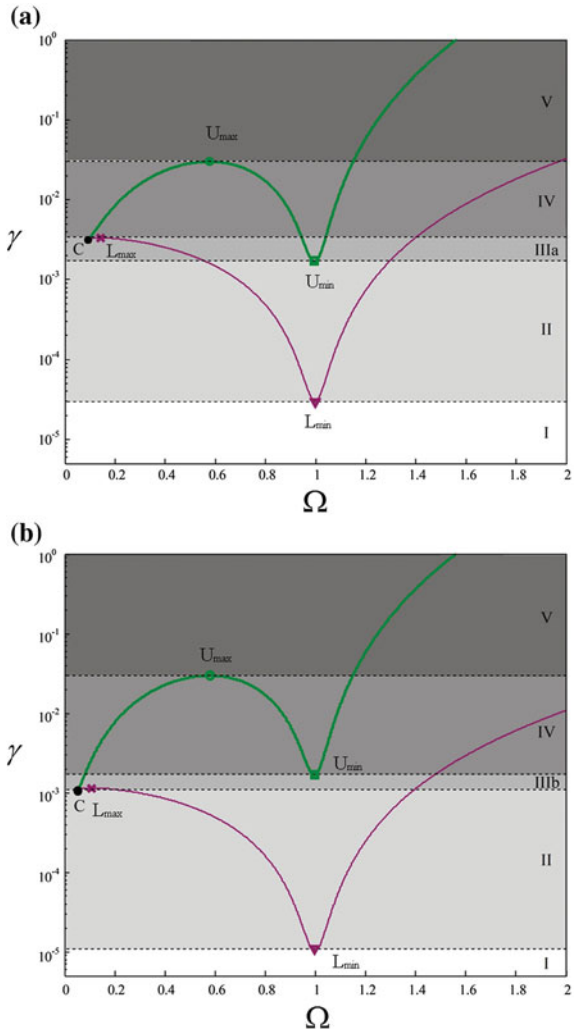

Fig. 11 Characteristic regions *I*–*V* in the $\Omega - \gamma$ plane, where the FRC of *W* exhibits different shapes, for $\zeta_s = 0.046$: **a** $\zeta = 0.026$; **b** $\zeta = 0.015$. Characteristic points U_{max}, L_{max}, U_{min}, L_{min} and C are also labelled

To emphasize the relationship between the bifurcation curves in the $\Omega - \gamma$ plane and the FRCs in the $\Omega - W$ plane, a three-dimensional plot involving the three variables Ω, γ, W is reported in Fig. 12. Two graphs are shown (Fig. 12a, b) to illustrate the relationship between the bifurcation curves in Fig. 11 and the FRCs of Figs. 7 and 8. It can be seen that a straight line, drawn for a particular value of γ, may be interpreted as the projection of the corresponding FRC on the $\Omega - \gamma$ plane. Moreover, the intersections between this straight line and the bifurcation curves give the values of the jump frequencies: jump-up points on the upper bifurcation curve, and jump-down points on the lower bifurcation curve.

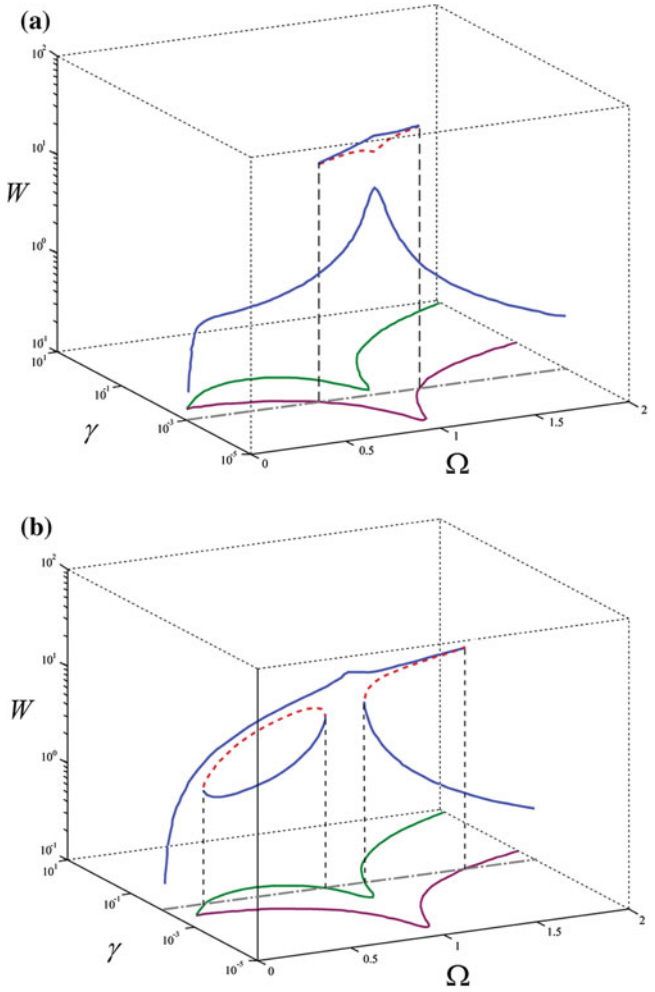

Fig. 12 Three-dimensional plot illustrating the relationship between the bifurcation curves and the FRCs

7 Summary

This chapter has presented an investigation into the dynamics of a nonlinear system attached to a shaker which is driven harmonically, where the mass of the nonlinear system is much less than that of the support structure and the shaker. Consequently, the nonlinear system has a negligible effect on the response of the shaker for the majority of frequencies. The stiffness nonlinearity of the attached system is due to the particular geometrical configuration of the elastic wires, represented as springs. The system has been modelled as a two degree-of-freedom system with a cubic type

nonlinearity and solved using the harmonic balance method to determine the primary frequency response equation and the stability conditions, which define the stable and unstable steady-state solutions. The system of equations has been decoupled and solved in closed-form. Good agreement has been found between the experimental results and the analytical and numerical solutions.

The effect of the system parameters on the frequency response curves was further investigated through simulations and it has been found that they can have different shapes. In particular, of main interest has been the case when the nonlinear attachment has a quasi-zero-stiffness. In this situation, closed detached resonance curves can appear. They can lie outside or inside the main resonance curve, and have stable and unstable parts. Approximate analytical expressions that define the boundaries between the shapes of the frequency response have been determined, enabling the parameters that influence the shape of the frequency response curves to be identified.

References

1. Nayfeh, A.H.: Nonlinear Interactions: Analytical Computational and Experimental Methods. Wiley, New York (2000)
2. Kovacic I, Brennan M.J. (eds): The Duffing Equation: Nonlinear Oscillators and Their Behavior. Wiley (2011)
3. Jiang, X., McFarland, M., Bergman, L.A., Vakakis, A.F.: Steady state passive nonlinear energy pumping in coupled oscillators: theoretical and experimental results. Nonlinear Dyn. **33**, 87–102 (2003)
4. Starosvetsky, Y., Gendelman, O.V.: Response regimes of linear oscillator coupled to nonlinear energy sink with harmonic forcing and frequency detuning. J. Sound Vib. **315**, 746–765 (2008)
5. Starosvetsky, Y., Gendelman, O.V.: Dynamics of a strongly nonlinear vibration absorber coupled to a harmonically excited two-degree-of-freedom system. J. Sound Vib. **312**, 234–256 (2008)
6. Starosvetsky, Y., Gendelman, O.V.: Vibration absorption in systems with a nonlinear energy sink: nonlinear damping. J. Sound Vib. **324**, 916–939 (2009)
7. Alexander, N.A., Schilder, F.: Exploring the performance of a nonlinear tuned mass damper. J. Sound Vib. **319**, 445–462 (2009)
8. Brennan, M.J., Gatti, G.: The characteristics of a nonlinear vibration neutralizer. J. Sound Vib. **331**, 3158–3171 (2012)
9. Hamdan, M.N., Burton, T.D.: On the steady state response and stability of non-linear oscillators using harmonic balance. J. Sound Vib. **166**, 255–266 (1993)
10. Worden, K.: On jump frequencies in the response of the Duffing oscillator. J. Sound Vib. **198**, 522–525 (1996)
11. Brennan, M.J., Kovacic, I., Carrella, A., Waters, T.P.: On the jump-up and jump-down frequencies of the Duffing oscillator. J. Sound Vib. **318**, 1250–1261 (2008)
12. Gatti, G., Kovacic, I., Brennan, M.J.: On the response of a harmonically excited two degree-of-freedom system consisting of a linear and a nonlinear quasi-zero stiffness oscillator. J. Sound Vib. **329**, 1823–1835 (2010)
13. Gatti, G., Brennan, M.J.: On the effects of system parameters on the response of a harmonically excited system consisting of weakly coupled nonlinear and linear oscillators. J. Sound Vib. **330**, 4538–4550 (2011)